PERGAMON

Journal of Structural Geology 22 (2000) 43–57

JOURNAL OF STRUCTURAL GEOLOGY

www.elsevier.nl/locate/jstrugeo

Fracture spacing in layered rocks: a new explanation based on the stress transition

Taixu Bai*, David D. Pollard

Department of Geological and Environmental Sciences, Stanford University, Stanford, CA 94305-2115, USA

Received 8 February 1999; accepted 17 August 1999

Abstract

Opening-mode fractures (joints and veins) in layered sedimentary rocks often are periodically distributed with spacings linearly related to the thickness of the fractured layer. To better understand this linear relation, we have investigated the stress distribution between two adjacent opening-mode fractures as a function of the fracture spacing to layer thickness ratio using a three-layer elastic model with a fractured central layer. The results show that when the fracture spacing to layer thickness ratio changes from greater than to less than a *critical value* (approximately 1.0) the normal stress acting perpendicular to the fractures changes from tensile to compressive. This stress state transition precludes further infilling of fractures unless there are existing flaws and/or the fractures are driven by an internal fluid pressure or other mechanisms. Hence, for fractures driven by tectonic extension, the critical fracture spacing to layer thickness ratio defines a lower limit, which also defines the condition of *fracture saturation*. The critical value of the fracture spacing to layer thickness ratio is independent of the average strain of the fractured layer, and it increases with increasing ratio of Young's modulus of the fractured layer to that of the neighboring layers. The critical value increases with increasing Poisson's ratio of the fractured layer, and with increasing overburden stress (depth), but it decreases with increasing Poisson's ratio of the neighboring layers. For representative variation of the elastic constants of the fractured layer and the neighboring layers, and overburden stress, the critical fracture spacing to layer thickness ratio varies between 0.8 and 1.2. This range encompasses the often cited spacing to layer thickness ratios in the literature for *well-developed* fractures sets.

1. Introduction

Opening-mode fractures (joints and veins) in layered sedimentary rocks are often confined by the layer boundaries with their height equal to the layer thickness (Helgeson and Aydin, 1991; Gross and Engelder, 1995). Fractures of the same set form under the same tectonic stress field and are parallel or subparallel to each other (Pollard and Aydin, 1988). In field observations, the spacing of two adjacent members of the same set is commonly measured as the distance between the fractures along a line perpendicular to the average orientation of the fracture set (Narr and Suppe, 1991; Gross, 1993).

Although there are some exceptions, many field observations reveal that fracture spacing in layered sedimentary rocks is roughly proportional to the thickness of the fractured layer with the ratio of spacing to layer thickness ranging from less than 0.1 to greater than 10 (Bogdanov, 1947; Novikova, 1947; Kirillova, 1949; Price, 1966; McQuillan, 1973; Narr and Lerche, 1984; Huang and Angelier, 1989; Narr and Suppe, 1991; Gross, 1993; Gross et al., 1995; Wu and Pollard, 1995; Becker and Gross, 1996; Ji and Saruwatari, 1998). The adverb 'roughly' is used here because none of the reported plots of fracture spacing versus layer thickness exactly follows a straight line. Instead the data are scattered to some extent about a 'best-fitting' line. In describing this rough linear relationship, mean (e.g. Huang and Angelier, 1989) or median (e.g. Narr and Suppe, 1991; Gross, 1993; Ji and Saruwatari, 1998) fracture spacing is usually used, and two terms,

* Corresponding author. Fax: +1-650-725-0979.
E-mail address: bai@pangea.stanford.edu (T. Bai)

0191-8141/00/$ - see front matter
PII: S0191-8141(99)00137-6

Fracture Spacing Ratio (FSR, Gross, 1993) and Fracture Spacing Index (FSI, Narr and Suppe, 1991), are introduced. FSR is the ratio of layer thickness to median fracture spacing for an individual layer. FSI is the slope of the best-fit line on plots of layer thickness versus median fracture spacing for a number of layers of varying thicknesses. The relative magnitudes of FSR and FSI are indicators of fracture density.

In this study, we investigate spacing of fractures formed during the extension of layered rocks using the finite element method (FEM). For simplicity, we postulate that the fractures are confined in a single mechanical layer (Narr and Suppe, 1991; Gross, 1993), are equally spaced, and may be modeled in two dimensions (i.e. in a cross-section view). In this case, the mean or median spacing is the same as the spacing between adjacent fractures. Also we use the term fracture spacing to layer thickness ratio to describe the linear relationship between spacing and layer thickness instead of FSR and FSI. This is because the focus is on fracture spacing rather than on fracture density. The spacing to layer thickness ratio is the inverse of FSR or FSI for the model configuration.

One process of joint formation in layered rocks has been described as 'sequential infilling' (Gross, 1993). This process is essentially that proposed by Hobbs (1967) and has been demonstrated in four-point bending experiments with brittle coating materials (Wu and Pollard, 1992, 1995). These experiments showed that as the remote strain increases the fracture spacing decreases approximately as the inverse of the remote strain, by fractures nucleating and propagating between earlier formed fractures. Eventually the fractures reach such a close spacing that no more fractures can infill, even with increasing strain. Instead, the existing fractures continue to open to accommodate the applied strain. This phenomenon is called 'fracture saturation' (Wu and Pollard, 1995). Similar terms were proposed in the geological literature, such as 'saturation model' by Cobbold (1979), and 'saturated with joints' by Narr and Suppe (1991), based on field observations; 'saturation of cracking' by Wu and Pollard (1991), and 'saturation level' by Rives et al. (1992), from experimental observation. Experimental work reported in the engineering literature shows a similar process for cross-ply laminates of glass-fibre-reinforced polyester (Garrett and Bailey, 1977a, b; Parvizi and Bailey, 1978).

Presently, none of the existing theoretical models (e.g. Lachenbruch, 1961; Hobbs, 1967; Cherepanov, 1997) can adequately account for fracture saturation and the range of spacing to layer thickness ratios from field observations. To better understand the linear relationship between fracture spacing and layer thickness, and to explain fracture saturation, we present a new theoretical model, which is the focus of this paper.

We first give a brief review of the previous theoretical models in the study of fracture spacing. We then investigate the stress state between adjacent fractures in a row of parallel equally spaced fractures in a layered material as a function of the average applied strain, the fracture spacing to layer thickness ratio, the overburden stress, and the elastic constants of the fractured layer and its neighboring layers using the FEM. Next, a laboratory experimental verification of the numerical results is introduced. Finally, the implications of the results for the study of fracture spacing in layered rock is discussed.

2. Previous theoretical models

One of the earliest theoretical explanations of the linear relation between fracture spacing and layer thickness was proposed by Hobbs (1967). Based on Cox's (1952) *stress transfer model*, Hobbs (1967) derived a linear relation between joint spacing and layer thickness with the coefficient depending upon the Young's modulus of the fractured layer, E_f, and the shear modulus of the neighboring layers, G_n. Specifically, for a given average strain (ε_{ave}) in the neighboring layers, the fracture spacing to layer thickness ratio (S/T_f) is

$$\frac{S}{T_f} = \left(\frac{1}{2}\right)^n \left(\frac{E_f}{G_n}\right)^{1/2} \cosh^{-1}\left(\frac{\varepsilon_{ave}}{\varepsilon_{ave} - \varepsilon_T}\right), \quad (1)$$

where ε_T is the maximum tensile strain in the fractured layer given by the ratio σ_T/E_f, with σ_T being the tensile strength of the fractured layer. The integer $n = 0$ just before fracturing between two joints as the stress at the midpoint approaches σ_T. Immediately after this first episode of infilling, $n = 1$, and the stress drops. Subsequent increase in ε_{ave}, according to Hobbs, would lead to another episode of infilling and a halving of S/T_f. In other words, as strain increases, spacing decreases *ad infinitum*. This model fails to explain fracture saturation and is inconsistent with the field observations (Narr and Suppe, 1991) and the experimental results (Garrett and Bailey, 1977a, b; Parvizi and Bailey, 1978; Wu and Pollard, 1995).

Conceptually, the three layers of the Hobbs' model are subjected to the same extension, but the stress falls to zero at the fracture surfaces in the middle layer. Stress is transferred from the intact neighboring layers to the region between the fractures. Once the stress midway between two adjacent fractures reaches the tensile strength of the rock in the fractured layer, as a result of increasing the average strain, new fractures are induced and the spacing is reduced by a factor of

1/2. Similar considerations have been used in the study of joints (Ji and Saruwatari, 1998), boudinage (Lloyd et al., 1982; Masuda and Kuriyama, 1988; Masuda et al., 1989, 1990), and the strength of rocks with rigid inclusions dispersed in a soft ductile matrix ('two-phase rocks', Ji and Zhao, 1994). Although the stress transfer concept has considerable merit, the stress distribution derived by Hobbs (1967) does not satisfy the fundamental equations of equilibrium and therefore violates conservation of momentum: it is not a possible stress distribution (see Appendix).

A similar explanation of fracture spacing is based on the concept of a *stress shadow* caused by the opening of a fracture (Lachenbruch, 1961; Nur, 1982; Pollard and Segall, 1987; Gross et al., 1995). At the fracture faces, the local fracture-normal stress is zero in the absence of fluid pressure within the fracture. This stress increases with increasing distance from the fracture and eventually reaches the remote value. Within a certain range of reduced stress, new fractures cannot form because the stress level is below the fracture stress of the rock, thereby defining a minimum spacing for a given loading.

A simple example of the stress shadow is based on the two-dimensional plane strain solution for the elastic boundary value problem of an opening-mode fracture in a homogeneous isotropic medium subjected to constant remote stress in the direction perpendicular to the fracture (Pollard and Segall, 1987). The minimum spacing between any two fractures is determined by the distance from the fracture at which the fracture normal stress returns to a specific percentage, C, of the remote value, and this distance is proportional to the fracture dimension that equals the mechanical layer thickness. Specifically the relation is

$$\frac{S}{T_f} = \frac{1}{2}\frac{C^{1/3}}{\sqrt{1-C^{2/3}}}. \quad (2)$$

As indicated by Pollard and Segall (1987), with $C = 99\%$, we have $S/T_f = 6.1$; and with $C = 72\%$, $S/T_f = 1.0$. It is possible that new fractures form at or beyond these distances. Therefore, the stress shadow concept helps explain the linear relation between fracture spacing and layer thickness, but the arbitrary nature of C precludes a specific application to fracture spacing.

Sowers (1972) and Cherepanov (1997) proposed that the periodic fracture patterns in layered rocks are caused by achieving a *limiting equilibrium state* (Timoshenko, 1936; Biot, 1965; Cherepanov, 1997) in the fractured layer. The concept is similar to the well-known phenomenon of buckling of a rod under axial compression. In layered materials, a compressive stress perpendicular to the layer causes the strain energy in the fractured layer (Sowers, 1972) and the compressive stress along the layer boundaries (Cherepanov, 1997) to be periodically distributed. These authors hypothesize that the periodic stress or strain energy distribution in the layer causes fractures to form selectively at locations of maxima in these quantities and in the direction perpendicular to the layer boundaries. Whereas Sowers (1972) used a numerical approach to solve the problem, Cherepanov (1997) solved the pro-

Table 1
Fracture spacing to layer thickness data from the literature

	Fracture spacing to layer thickness ratio (S/T_f)[a]	Reference
Range IV	< 0.1	Ladeira and Price (1981)
	< 0.1	Ladeira and Price (1981)
	< 0.1	Ladeira and Price (1981)
	0.11	Becker and Gross (1996)
	0.17	Ladeira and Price (1981)
	0.23	Ladeira and Price (1981)
Range III	0.31	Ladeira and Price (1981)
	0.41	Gross et al. (1995)
	0.42	Ladeira and Price (1981)
	0.44	Gross et al. (1995)
	0.45	Gross et al. (1997)
	0.56	Gross (1993)
	0.59	Price (1966)
	0.60	Huang and Angelier (1989)
	0.67	Gross et al. (1997)
	0.71	Gross et al. (1997)
	0.74	Gross et al. (1997)
	0.76	Narr and Suppe (1991)
	0.76	Gross (1993)
	0.77	Gross et al. (1997)
	0.77	Becker and Gross (1996)
	0.79	Narr and Suppe (1991)
	0.79	Gross (1993)
	0.79	Gross (1993)
Range II	0.81	Gross (1993)
	0.82	Narr and Suppe (1991)
	0.83	Gross et al. (1997)
	0.83	Ji and Saruwatari (1998)
	0.90	Gross et al. (1995)
	0.92	Gross et al. (1995)
	0.95	Gross et al. (1997)
	1.00	Gross et al. (1997)
	1.05	Huang and Angelier (1989)
	1.05	Gross et al. (1997)
	1.05	Gross et al. (1997)
	1.06	Wu and Pollard (1995)
	1.11	Gross et al. (1997)
	1.11	Price (1966)
	1.11	Price (1966)
	1.18	Gross et al. (1997)
Range I	1.25	Becker and Gross (1996)
	1.47	McQuillan (1973)
	1.47	Gross (1993)
	1.67	Ladeira and Price (1981)
	2–10	Narr and Suppe (1991)

[a] Note the spacing to layer thickness ratios in this table were calculated using the inverse of the Fracture Spacing Index (FSI) or the Fracture Spacing Ratio (FSR). Different spacing to layer thickness ratios from the same author(s) are from different layers.

blem analytically. In terms of the fracture spacing to layer thickness ratio, the following expression can be derived from Cherepanov's solutions

$$\frac{S}{T_f} = \frac{\sqrt{3}}{2}\frac{\pi}{\sqrt{(1+\nu_f)^2 - 3\nu_f}}, \tag{3}$$

where ν_f is the Poisson's ratio of the fractured layer. This implies that the spacing to layer thickness ratio is only a function of the Poisson's ratio of the fractured layer. This is inconsistent with the field observations that spacing is a function of the stiffness of the fractured layer (Gross et al., 1995). Furthermore, for $\nu_f = 0$, we get $S/T_f = 2.72$; and for $\nu_f = 0.5$, we have $S/T_f = 3.14$. These cover only a few data sets from field observations (refer to Table 1).

3. Numerical modeling

3.1. Numerical method and boundary conditions

We investigate the stress state transition between adjacent equally spaced fractures using a two-dimensional finite element code named FRANC (FRacture ANalysis Code). This code was developed at Cornell University and is based on the theory of linear and non-linear elastic fracture mechanics (Wawrzynek and Ingraffea, 1987). The model, its boundary and loading conditions, and the FEM mesh are shown in Fig. 1. The mesh was refined by reducing the sizes of the elements until calculated stresses differed by less than 0.2% in the central layer. The fractured central layer has a thickness $T_f = 0.2$ m, which is also the height of the fractures (H). The overall thickness of the model ($T = T_f + 2T_n$) is 0.8 m. The model width (W) varies according to the spacing of fractures such that the distance from the left (or right) boundary to the left-most (or right-most) fracture is at least three times the fracture height. For this layered model, we postulate the two materials across the layer boundaries are welded together, i.e. no slip or opening is permitted along the layer boundaries, and we postulate a plane strain condition for the entire model. The Young's moduli and Poisson's ratios for the adjacent layers are the same, E_n and ν_n, but may differ in the layer containing the fractures, E_f and ν_f.

We fix the whole bottom boundary of the model in the y-direction, $u_y(B) = 0$, and the middle point of the bottom boundary in the x-direction as well, $u_x(B) = 0$ at $x = 0$. We use a constant displacement condition in the x-direction along the left boundary, $u_x(L) = -U_x$, and the right boundary, $u_x(R) = U_x$. The left and right boundaries are not constrained in the y-direction except at their lower corners. The top boundary is free to displace as necessary to produce the designated values of average strain in the x-direction for the study of the average strain effect, and the elastic constant effect on the critical spacing to layer thickness ratio (see below). The average strain in the x-direction, ε_{xx}(ave), is calculated as

$$\varepsilon_{xx}(\text{ave}) = 2U_x/W. \tag{4}$$

In the study of overburden effects on the critical spacing to layer thickness ratio, we use a constant displacement in the y-direction along the top boundary, $u_y(T) = -U_y$. For the case where the elastic constants of the fractured layer and its neighboring layers are the same, the overburden stress (magnitude), S_v, can be calculated as

$$S_v = -\frac{E_f}{(1+\nu_f)(1-2\nu_f)}\left[\nu_f\varepsilon_{xx}(\text{ave}) - (1-\nu_f)\frac{U_y}{T}\right]. \tag{5}$$

In all of the models, we introduce only four fractures in the row because our numerical results (Bai et al., in press) with models containing up to 23 evenly spaced fractures show that only the end members behave significantly different from the other members. In terms of fracture aperture and stress distribution, all the members except those on the ends show nearly the same behavior with differences of less than 2%. This gives us the confidence to use the middle two fractures in the four-fracture model to represent any two adjacent fractures in a row composed of many equally spaced members.

3.2. Stress state transition and the critical spacing to layer thickness ratio

To show how the stress distribution varies as a function of the fracture spacing, we plot the distribution of the normal stress in the direction perpendicular to the fractures (σ_{xx}) versus the normalized position (x/T_f) along the line which is perpendicular to the fractures and bisects them (Fig. 1, line AA′) for different fracture spacing to layer thickness ratios (Fig. 2). Using the sign convention that tensile stress is positive, the stress distributions are calculated for models with the same elastic constants for the three layers (Young's moduli $E_f = E_n = 40$ GPa; Poisson's ratios $\nu_f = \nu_n = 0.2$) and an average normal strain across the entire model in the direction perpendicular to the fractures of $\varepsilon_{xx}(\text{ave}) = 0.002$. From the plot, we see that when the fracture spacing to layer thickness ratio is 0.9 and less, the stress is compressive (negative); whereas when the ratio is 1.0 and greater, the stress along the central portion of the plot changes to tensile (positive).

This result shows that there is a *critical value* for the fracture spacing to layer thickness ratio, which charac-

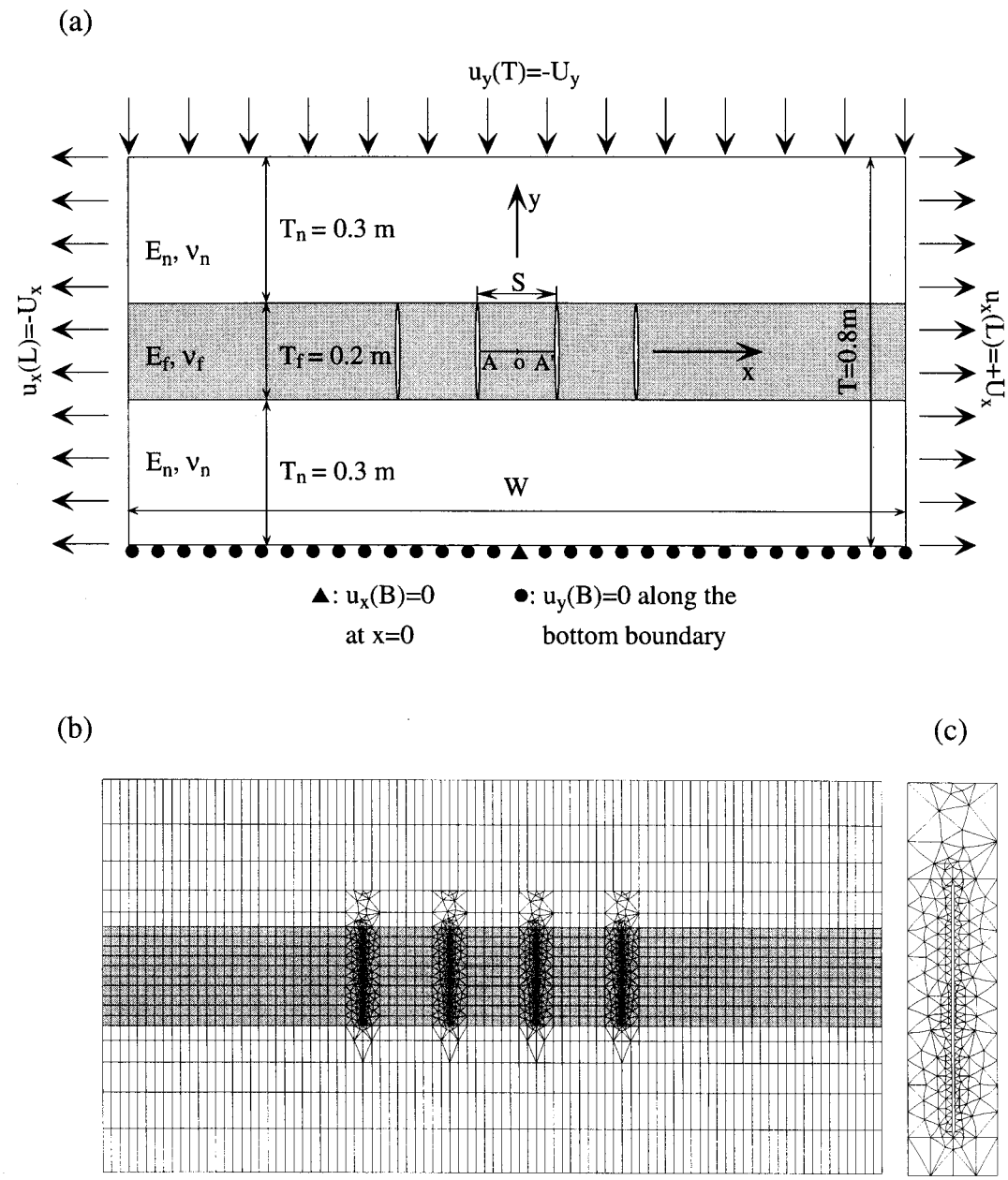

Fig. 1. (a) FEM model and its boundary conditions of layered rocks with four equally spaced fractures in the fractured layer. The x-axis is parallel to the layer boundaries and perpendicular to the fractures. The y-axis is perpendicular to the layer boundaries. The displacements imposed along the left and right boundaries are $u_x(L)$ and $u_x(R)$, respectively. The bottom boundary is fixed in the y-direction, with the middle point fixed in the x-direction as well. A displacement $u_y(T)$ is imposed on the top boundary of the model to simulate the effect of overburden stress. See text for details. (b) The FEM mesh of the entire model. (c) The mesh around one of the fractures.

terizes a stress state transition between the two fractures: when the ratio is above this critical value the stress is tensile in the central part along line AA′ (refer to Fig. 1), whereas below this critical value the stress is compressive all along the line. We call this the *critical spacing to layer thickness ratio*, $(S/T_f)_{cr}$. The sign of the stress at the central point of line AA′ (i.e. point o in Fig. 1) is used to define the transition: when the sign of the stress at point o is positive, the corresponding spacing to layer thickness ratio is above the critical value; otherwise the corresponding spacing to layer thickness ratio is below the critical value. For the case with the same elastic constants for all three layers, the critical ratio lies between 0.9 and 1.0.

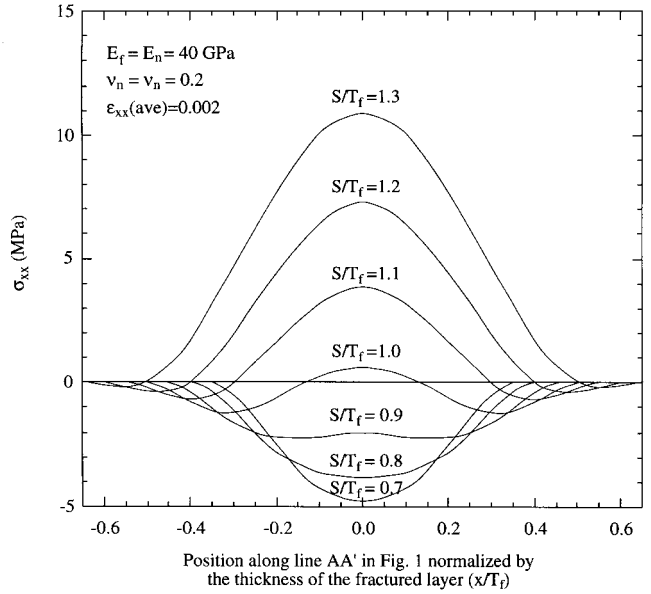

Fig. 2. Distributions of the normal stress component in the direction perpendicular to the fractures (σ_{xx}) along the line AA′ (refer to Fig. 1) as a function of fracture spacing to layer thickness ratio (S/T_f). The figure shows that there is a critical spacing to layer thickness ratio between 0.9 and 1.0, which marks the stress state transition. When the spacing to layer thickness ratio (S/T_f) is less than the critical value, the stress is compressive; whereas, when it is greater than the critical value, the stress in the middle of the plot line becomes tensile.

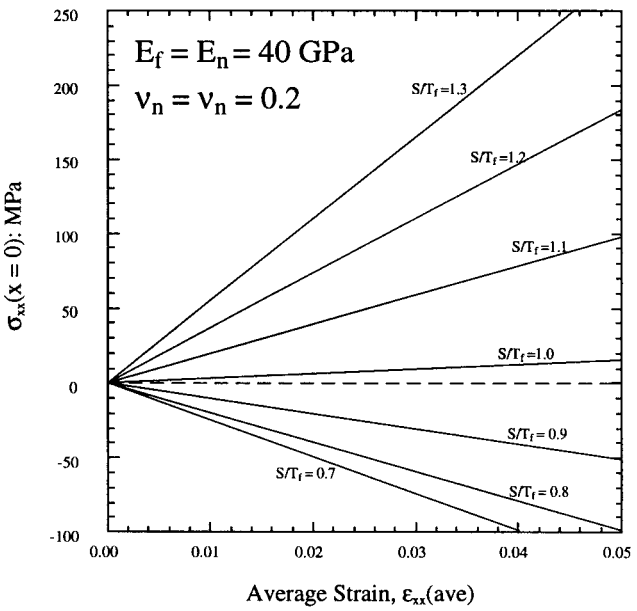

Fig. 3. Plots of the normal stress in the direction perpendicular to the fractures, σ_{xx}, at point o (refer to Fig. 1) as a function of average strain, ε_{xx}(ave), at various fracture spacing to layer thickness ratios (S/T_f). The stress is linearly related to the average strain. So the average strain does not affect the value of the critical spacing to layer thickness ratio.

3.3. Effects of loading (average strain) on the critical fracture spacing to layer thickness ratio

As shown in Fig. 3, values of $\sigma_{xx}(x = 0)$ are linearly related to the average strain with the slope depending upon the spacing to layer thickness ratio. In other words, the average strain only affects the magnitude of $\sigma_{xx}(x = 0)$ but not its sign. The critical spacing to layer thickness ratio is independent of the average strain, and therefore independent of the displacement boundary conditions that provide the average strain for the model.

3.4. Effects of the elastic constants on the critical fracture spacing to layer thickness ratio

The critical ratio, $(S/T_f)_{cr}$, determined as either the Young's modulus of the fractured layer or that of the neighboring layers, is varied, while keeping the other elastic properties constant (Fig. 4a). The critical spacing to layer thickness ratio increases with increasing Young's modulus of the fractured layer (E_f), but decreases with increasing Young's modulus of the neighboring layers (E_n).

By plotting the critical spacing to layer thickness ratio versus the ratio of the Young's moduli (E_f/E_n), we obtain the unique relation shown in Fig. 4(b). The critical spacing to layer thickness ratio is non-linearly related to the ratio of the Young's moduli (E_f/E_n): a sharp change of the critical spacing to layer thickness ratio occurs in the range of $0 < E_f/E_n < 2.0$ (Fig. 4). As this ratio goes to infinity, the critical spacing to length ratio asymptotically approaches 1.12, which is evaluated at $E_f/E_n = 4000$. The best fit line to the numerical results can be expressed as

$$(S/T_f)_{cr} = 0.792 + 0.328\{1 - \exp[-0.824(E_f/E_n - 0.0025)^{0.824}]\}. \quad (6)$$

The overall variation of the critical spacing to layer thickness ratio caused by changes in the Young's moduli in the plotted range is approximately 32%. This variation can be further constrained by considering the fact that the stiffer bed is more likely to be fractured during tectonic extension. As two examples among many others for relative stiffness of the fractured layer and the neighboring layer, (1) Helgeson and Aydin (1991) observed that in interbedded limestone and shale sequences joints are found in limestone layers but not in the shale layers; (2) Gross et al. (1995) described the siliceous units from the Monterey

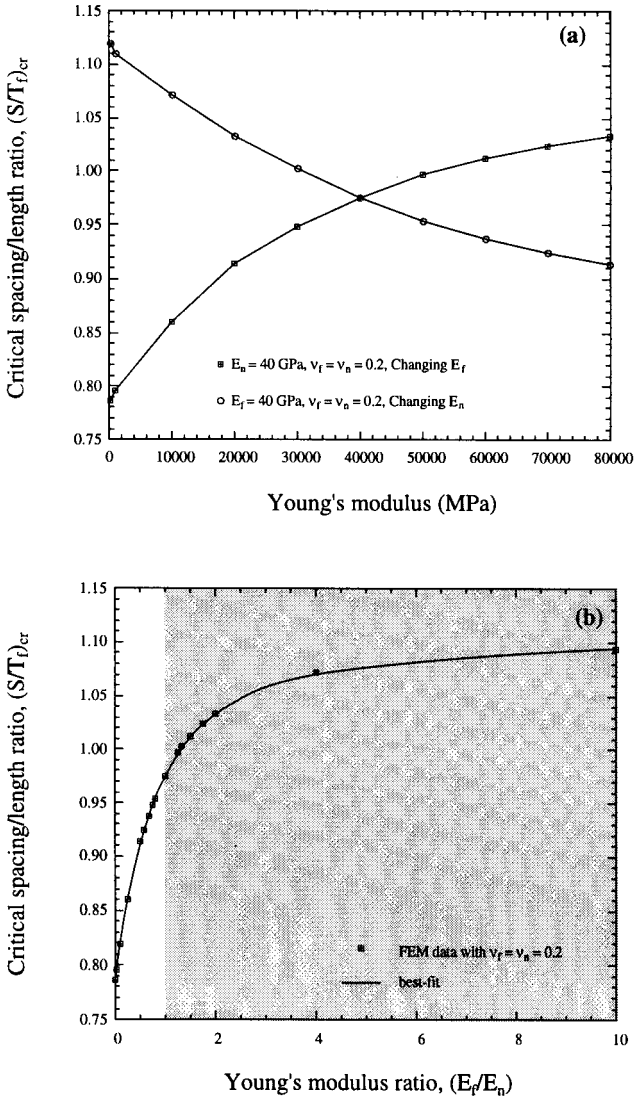

Fig. 4. The Young's modulus effects on the critical fracture spacing to layer thickness ratio, $(S/T_f)_{cr}$. (a) The critical spacing to layer thickness ratio increases with increasing Young's modulus of the fractured layer (E_f), but it decreases with increasing Young's modulus of the neighboring layers (E_n). (b) The critical spacing to layer thickness ratio increases with increasing Young's modulus ratio (E_f/E_n).

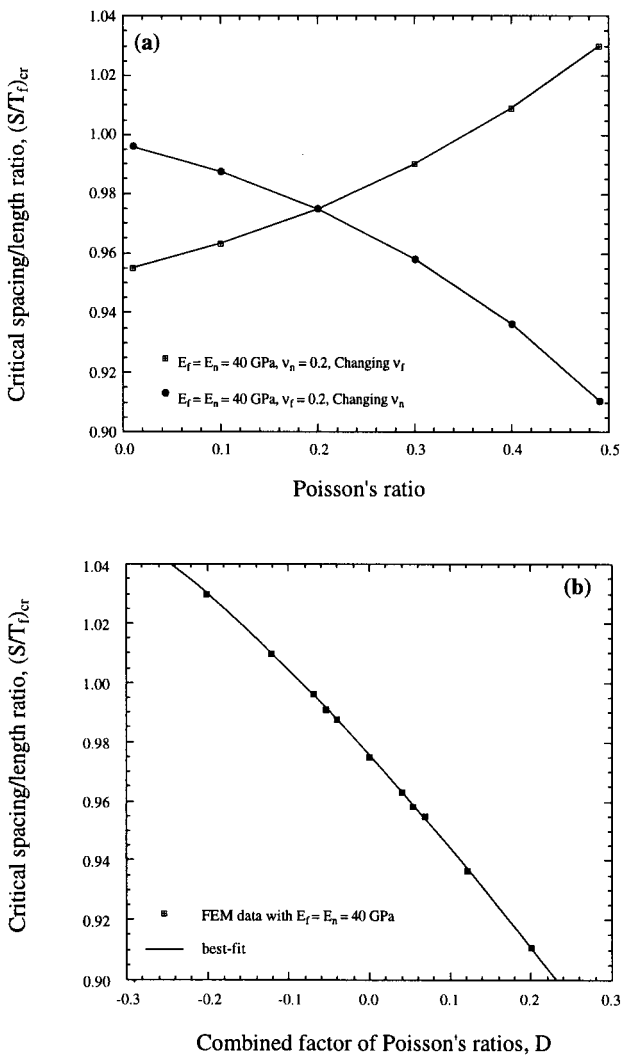

Fig. 5. The Poisson's ratio effects on the critical fracture spacing to layer thickness ratio, $(S/T_f)_{cr}$. (a) Plots show that $(S/T_f)_{cr}$ increases with increasing Poisson's ratio of the fractured layer, but it decreases with increasing Poisson's ratio of the neighboring layers. (b) The relation between $(S/T_f)_{cr}$ and a combined factor of the Poisson's ratios, $D = [(1-2\nu_f)(1+\nu_f)-(1-2\nu_n)(1+\nu_n)]/[(1-\nu_f^2)+(1-\nu_n^2)]$.

Formation as being full of joints, but no joint is found in the neighboring clay-rich units. We conclude that in most cases the jointed layer is stiffer than the neighboring layers. That is, $E_f/E_n \geq 1$ (shaded area in Fig. 4b). Hence we reduce the overall variation of the critical spacing to layer thickness ratio to about 12%. Young's moduli of sedimentary rocks vary from 0.125 GPa for poorly cemented siltstone to 103 GPa for jaspillite, ferrugtinous, and silicious sandstone (Hatheway and Kiersch, 1989). This gives the maximum Young's modulus ratio of 824. However, for most sedimentary rocks, Young's moduli fall within the range of 5–80 GPa. Furthermore, as the ratio of the Young's moduli increases beyond the plot range in Fig. 4(b), the slope of the curve becomes flat. The relative variation of the critical spacing to layer thickness ratio is within 12% even when the Young's modulus ratio is 1000.

The effects of the Poisson's ratios of the fractured layer and its neighboring layers on the value of the critical spacing to layer thickness ratio are considered by changing either Poisson's ratio of the fractured layer or that of the neighboring layers, while keeping the other elastic properties constant. The critical spacing to layer thickness ratio increases with increasing Poisson's ratio of the fractured layer (ν_f) and decreases

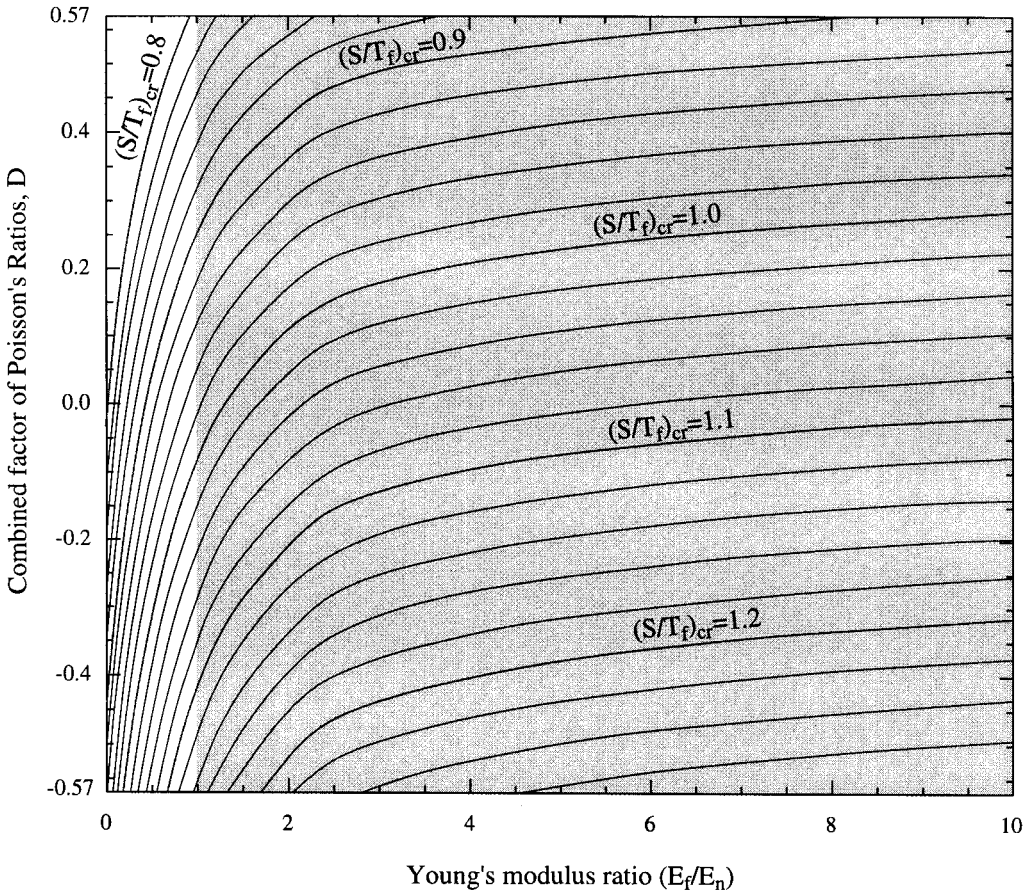

Fig. 6. The critical fracture spacing to layer thickness ratio $(S/L)_{cr}$ variation as a function of the Young's modulus ratio (E_f/E_n), and the combined factor from the Poisson's ratios (D). Shaded area shows the reasonable range.

with increasing Poisson's ratio of the neighboring layers (ν_n) (Fig. 5a). To understand the effects of Poisson's ratio, we plot (Fig. 5b) the critical spacing to layer thickness ratio versus a factor, D, defined as

$$D = \frac{(1-2\nu_f)(1+\nu_f)-(1-2\nu_n)(1+\nu_n)}{(1-\nu_f^2)+(1-\nu_n^2)}, \tag{7}$$

which is motivated by the Dundurs Parameter at $E_f = E_n$ (Dundurs, 1969; Barber, 1992). The plot shows that the critical spacing to layer thickness ratio decreases monotonically with increasing D. Their relation is approximated as

$$(S/T_f)_{cr} = 0.976 - 0.302D - 0.129D^2 + 0.117D^3. \tag{8}$$

The overall variation of the critical spacing to layer thickness ratio caused by the changes in Poisson's ratio is about 13%. The reported values of Poisson's ratio for sedimentary rocks vary from 0.01 for carboniferous sandstone to 0.46 for dolomite (Hatheway and Kiersch, 1989). The plot in Fig. 5(b) covers all the possible values of Poisson's ratio of sedimentary rocks.

We combine the effects of the Young's moduli and the Poisson's ratio on the critical fracture spacing to layer thickness ratio by multiplying (6) and (8) and normalizing the product by the value of $(S/T_f)_{cr}$ at $E_f = E_n = 40$ GPa, and $\nu_f = \nu_n = 0.2$, i.e. $(S/T_f)_{cr} = 0.976$. The combined relation can be written as

$$(S/T_f)_{cr} = \beta\big(0.792 + 0.328\{1 - \exp[-0.824 (\alpha - 0.0025)^{0.824}]\}\big), \tag{9}$$

where $\alpha = E_f/E_n$, and $\beta = (0.976 - 0.302D - 0.129D^2 + 0.117D^3)/0.976$. Fig. 6 shows the combined effects of the Young's moduli and the Poisson's ratio based on the relations shown in Eq. (9). Along each of the lines in this figure, the critical spacing to layer thickness ratio is a constant.

3.5. Effects of overburden on the critical fracture spacing to layer thickness ratio

Due to limitations of the finite element code, FRANC, we cannot use mixed stress–displacement

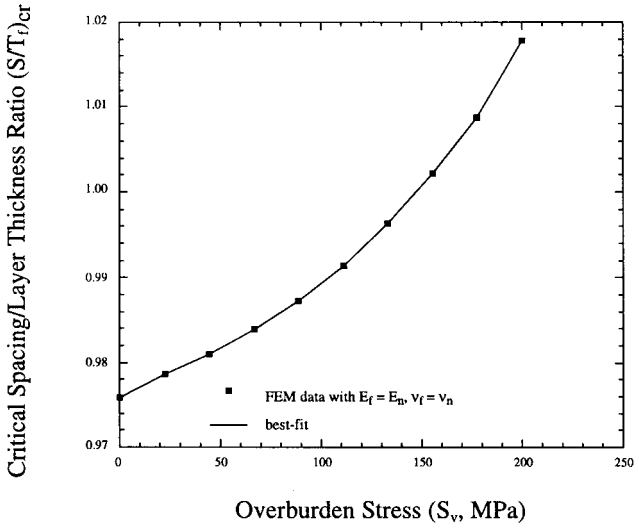

Fig. 7. Plot shows that the critical spacing to layer thickness ratio, $(S/T_f)_{cr}$, increases with increasing overburden stress, S_v.

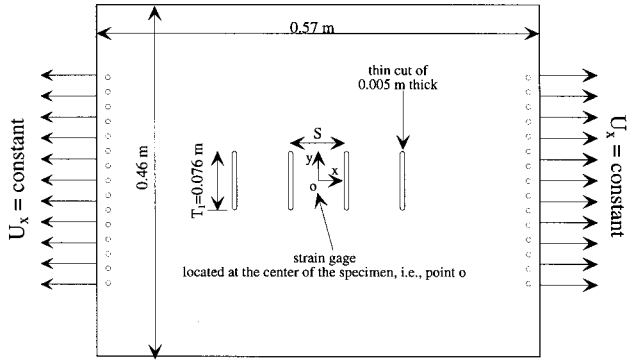

Fig. 8. Sketch of the experimental specimen and the finite element model used to verify the experimental results. The specimen is loaded by pinning it with the steel loading frame (not shown) through the holes near the left and right edges. The FEM model does not contain the pinholes, and the load is applied as constant displacements along the left and right boundaries.

boundary conditions. To simulate the overburden effect on the critical spacing to layer thickness ratio, while keeping all the other boundary conditions the same as before (Fig. 1a), we use constant displacement along the upper boundary of the model with a magnitude necessary to generate a stress field equivalent to that caused by the weight of overburden (see Eq. 5).

In modeling the overburden effect on the critical spacing to layer thickness ratio, we use $E_f = E_n = 40$ GPa, $\nu_f = \nu_n = 0.2$, $\varepsilon = 0.002$, and vary U_y to generate overburden stress of magnitudes ranging from 0 to 200 MPa. We plot the critical spacing to layer thickness ratio versus overburden stress in Fig. 7. The plot shows that the critical spacing to layer thickness ratio increases with increasing overburden stress. The relationship is

$$(S/T_f)_{cr} = a + bS_v + cS_v^2 + dS_v^3, \tag{10}$$

where $a = 0.976$, $b = 1.118 \times 10^{-4}$, $c = -7.562 \times 10^{-8}$, and $d = 2.806 \times 10^{-9}$.

The overall variation of the critical spacing to layer thickness ratio caused by the overburden stress is less than 5%. This is smaller than the variations caused by the range of elastic constants. The range of the overburden stress in the plot corresponds approximately to depth ranging from 0 to 8 km.

To accommodate the overburden effect on the critical spacing to layer thickness ratio, we rewrite Eq. (10) as

$$(S/T_f)_{cr} = \beta\gamma\big(0.792 + 0.328\{1 - \exp[-0.824 (\alpha - 0.0025)^{0.824}]\}\big), \tag{11}$$

where $\gamma = (a + bS_v + cS_v^2 + dS_v^3)/0.976$. Eq. (11) gives the general expression of the critical spacing to layer thickness ratio as a function of the elastic constants of the fractured layer and those of the neighboring layers, and the overburden stress.

4. Experimental verification

We used Plexiglas (PMMA) plate specimens of dimensions as shown in Fig. 8 to verify our numerical results. The material has elastic constants $E = 31$ GPa and $\nu = 0.36$ (Wu and Pollard, 1992). The specimens were loaded on a custom-built servo-controlled biaxial loading machine and the vertical and horizontal strain at the center points of the specimens (point o, Fig. 8) were measured with biaxial strain rosettes (WA-06-120WT-350, manufactured by M&M Measurement Group, INC.). A Vishay P-3500 digital strain indicator and a Vishay switch and balance unit were used in the strain measurement. The plates are homogeneous, so T_f is taken as the height of the cuts, and $E_f = E_n$, $\nu_f = \nu_n$. The experimental strain versus the average strain across the plate for different S/T_f ratios are plotted as discrete points in Fig. 9.

We constructed numerical models with the same dimensions, elastic constants, and boundary conditions as the experimental specimens. Because the PMMA plates are thin (0.005 m), we postulate plane stress conditions for the numerical models. The numerical results are plotted as lines in Fig. 9. For all the specimen configurations, the strain at point o (refer to Fig. 8) is linearly related to the average strain. Furthermore, the experimental strain magnitudes are similar to, but are systematically less than the FEM strain magnitudes, with differences ranging from 10 to 25 microstrains.

Several explanations may account for the small sys-

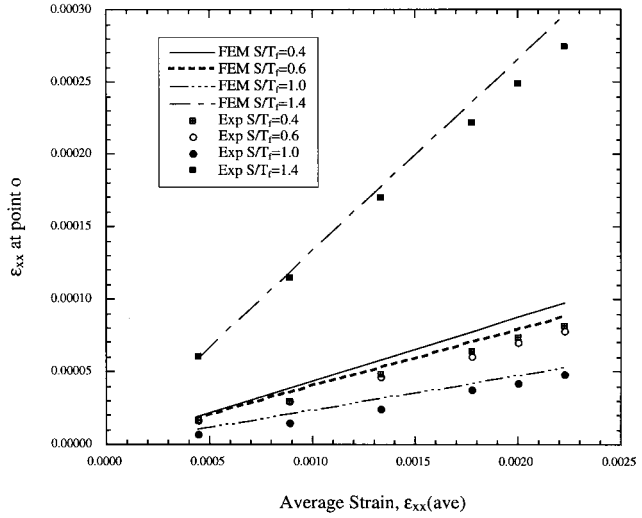

Fig. 9. Comparison of the normal strain in x-direction at point o (refer to Fig. 8) from the experiments and those from the FEM modeling. Results from both the experiments and the FEM modeling show that the strain at point o increases linearly with increasing average strain, ε_{xx}(ave). The discrepancies between the experimental and FEM results range from 10 to 25 microstrains.

tematic discrepancy between the numerical and laboratory experiments shown in Fig. 9. First, the maximum error in strain measurement with the experimental setup is about 5 microstrains. Second, the FEM strain was obtained at point o (see Fig. 8), whereas the experimental strain was the average strain across the length of the strain gage. Averaging the FEM strain across the same length as the strain gage accounts for about 2–3 microstrain of the discrepancy. Third, in doing the experiments, specimens were loaded by pinning them with a steel loading frame through holes close to their left and right boundaries (Fig. 8), whereas the numerical models were loaded with displacement boundary conditions right at the corresponding boundaries, and the numerical models do not contain any pinholes. Thus, the experimental specimens deform more (perhaps also inelastically) close to the pinholes and less far away from them. This causes the average strain across the central area of the experimental specimens to be systematically less than that of the FEM models. We consider this to be the major source for the discrepancy between the experimental and FEM strains. However, the exact contribution of this source to the discrepancy is difficult to evaluate.

One may consider that the elastic constants assigned to the numerical models may not be the same as those of the experimental specimen, and this may contribute to the discrepancy shown in Fig. 10. To examine whether this is true, we have varied the elastic constants in the FEM models. The results show that the strain solutions are independent of the elastic constants, so the differences between the elastic constants

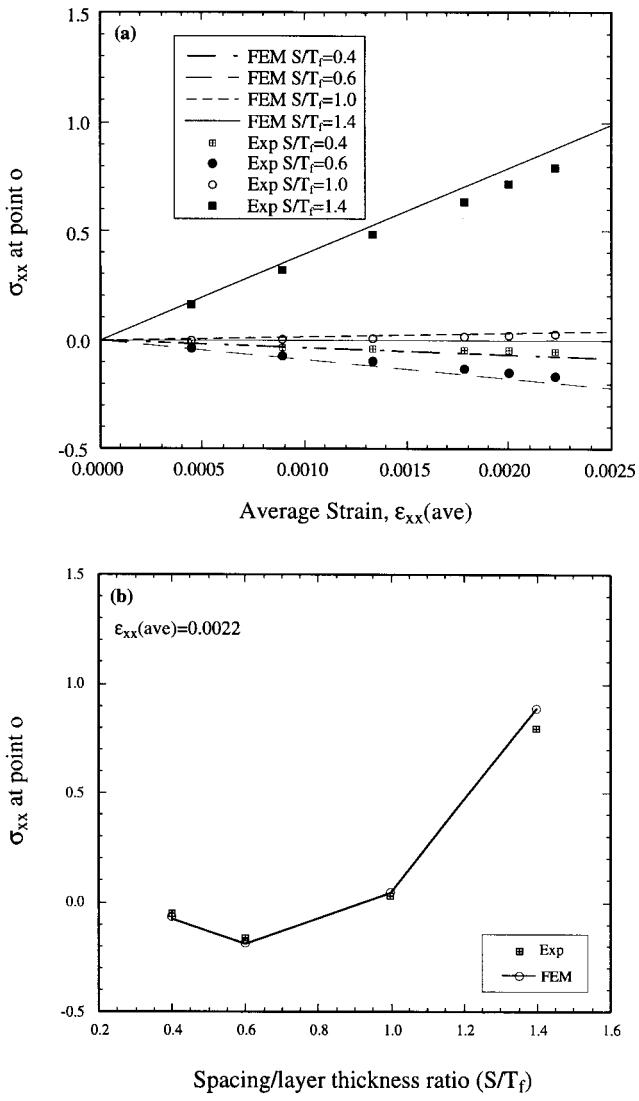

Fig. 10. Results of the normal stress in x-direction at point o from the experiments and the same stress from the FEM modeling (refer to Fig. 8). Results from both the experiments and the FEM modeling show that the stress at point o increases linearly with increasing average strain, ε_{xx}(ave). Also the stress is tensile when $S/T_f \geq 1.0$; whereas it is compressive when $S/T_f < 1.0$.

of the FEM models and those of the experimental specimens do not cause any discrepancy in the strains.

The measured strain data can be converted to stress using the equation,

$$\sigma_{xx} = \frac{E}{1-\nu^2}(\varepsilon_{xx} + \nu\varepsilon_{yy}), \tag{12}$$

derived from the two-dimensional statement of Hooke's Law for plane stress conditions (Jaeger and Cook, 1979). Eq. (12) implies that the stress state at point o is determined by the strain term $(\varepsilon_{xx} + \nu\varepsilon_{yy})$. Although ε_{xx} is extensional (positive, Fig. 9), the stress σ_{xx} can be either tensile (positive) or compressive

(negative), depending on the sign of $(\varepsilon_{xx} + \nu\varepsilon_{yy})$. For small ratios of spacing to fracture height, the strain in the y-direction is negative enough to induce a compressive stress.

The experimental stress versus the average strain for different S/T_f ratios are plotted in Fig. 10(a), and the experimental stress versus the S/T_f ratio for the case with $\varepsilon_{xx}(\text{ave}) = 0.0022$ is plotted in Fig. 10(b). Fig. 10(a) and (b) shows that when the experimental S/T_f ratio is 0.4 and 0.6, the stress (σ_{xx}) at point o is compressive. When the S/T_f ratio is 1.0 and 1.4, the stress at point o is tensile. These results agree with those for the stress transition found using the numerical modeling.

5. Discussion

In the previous sections, we show that there is a stress state transition between two adjacent opening-mode fractures in both a homogeneous material and a layered material under extension. In this section, we discuss the implications of the results to the process of jointing in layered rocks. Then, we summarize the field measurements of joint spacing from the literature and explain these data using our numerical results.

5.1. Mechanism of fracture saturation

Opening-mode fractures form in response to tensile stress in the direction perpendicular to the fracture plane and/or internal fluid pressure (Pollard and Aydin, 1988). The stress state transition described in this paper implies that an opening-mode fracture cannot form between two fractures with a spacing to layer thickness ratio less than the critical value unless a locally perturbed tensile stress field exists somewhere between the fractures (e.g. at flaw tips), or a mechanism (e.g. internal fluid pressure) exists to overcome the compressive stress. With these caveats, *the critical spacing to layer thickness ratio gives the lower limit for the spacing to layer thickness ratio, i.e. the ratio at fracture saturation*. The stress state transition provides an explicit mechanism for fracture saturation in layered rocks.

5.2. Joint spacing data from the literature

Field observations provide a broad range of fracture spacing to layer thickness ratios from less than 0.1 to greater than 10, with the most commonly reported values between 0.3 and 1.2 (see Table 1). Exceptions do exist. Narr and Suppe (1991) report that the fracture spacing to layer thickness ratio varies from 2 to 10 with structural position in the Monterey Formation. McQuillan (1973) and Ladeira and Price (1981) report spacing to layer thickness ratios of close to zero in Asmari limestone, Portuguese greywacke and UK greywacke layers with thickness greater than 1.5 m and up to 12 m. Becker and Gross (1996) report a joint spacing to layer thickness ratio of about 0.11 near a fault zone in a limestone layer of the Turonian Gerofit Formation, Southern Israel.

For convenience in the following discussion, we classify fracture spacing to layer thickness ratios into four ranges with

Range I: $S/T_f > 1.2$;

Range II: $0.8 \le S/T_f < 1.2$;

Range III: $0.3 \le S/T_f < 0.8$;

Range IV: $S/T_f < 0.3$.

5.3. Explanations for different joint spacings in layered rocks

The spacings in Range I ($S/T_f > 1.2$) can be explained as the jointing process in the beds having not reached the saturation level. The numerical experiments by Rives et al. (1992) show that each layer in a series of layers can have different levels of development. For a joint set in Range I, the measured mean joint spacing value is unlikely to be the minimum possible value for that layer. Because spacing in this range changes significantly for minor variations in applied strain (Wu and Pollard, 1995), measured values of spacing to layer thickness in Range I may be useful for characterizing the strain.

The spacings in Range II ($0.8 \le S/T_f < 1.2$) correspond to our critical spacing to layer thickness ratio (defined in Eq. 11), i.e. spacing at or near the saturation level. For a given fracture set, the critical spacing to layer thickness ratio is determined by the layer thickness, the Young's modulus ratio, the Poisson's ratios of the fractured layer and the neighboring layers, and the overburden stress during the formation of the fractures, but it is independent of the applied average strain (Fig. 3). Therefore, data on spacing to layer thickness ratios in Range II may not be used for strain characterization.

For the spacings in Ranges III and IV, the most prevalent explanations (e.g. Narr and Suppe, 1991; Rives et al., 1992; Gross, 1993; Becker and Gross, 1996) are versions of the concept proposed by Hobbs (1967). Later joints are said to form in the intervals between two earlier-formed adjacent joints as a result of the stress transferred from adjacent layers as the average strain increases. When the average strain reaches a certain value, either the tensile stress at the

middle point achieves the level of the tensile strength of the rock, or the stress intensity factor of any flaw between the two earlier-formed joints achieves the fracture toughness of the rock and a new fracture forms. Consequently, closely spaced joints are interpreted to have formed in localities where there is a high average strain magnitude.

However, our FEM and laboratory results imply that with only an extension of the layers, it is impossible to have new fractures form between two earlier fractures if the spacing to layer thickness ratio of the earlier fractures is equal to or less than the critical ratio, because the normal stress component in the direction perpendicular to the fractures is compressive (Fig. 2). This stress component as derived by Hobbs is tensile for all spacing to layer thickness ratios, but the Hobbs stress distribution does not satisfy the equilibrium equations of elasticity (see Appendix). Therefore, some new mechanisms must be considered to overcome the compressive stress and thereby explain the formation of closely spaced fractures.

A possible mechanism is that the compressive stress between two fractures is overcome by the local tensile stress produced where flaws exist in the fractured layer. The compressive overburden stress in the direction parallel to the joints could produce tensile stress in the direction perpendicular to the joints if the flaws have a finite radius of curvature at their upper or lower extremity (Pollard and Aydin, 1988, fig. 20). The magnitude of this tensile stress would increase with depth, and it would increase with internal fluid pressure in the flaw.

We conclude that fractures with spacing in Range III and IV could form at depth in the crust under the action of overburden load and/or fluid pressure, if such flaws exist. Under these conditions the explanation of fracture saturation due to the stress transition breaks down. Field evidence for infilling joints initiating at flaws with finite radii of curvature would be diagnostic of this mechanism.

Flaws may be cracks of various lengths and these may be located at the layer interfaces or in the middle of the fractured layer, as observed by Helgeson and Aydin (1991). In a companion paper, we study the process of sequential infilling by crack-like flaws between existing fractures with spacing to layer thickness ratio less than the critical value. The results show that existing flaws of certain sizes can significantly change the local stress field, i.e. a crack can propagate into and through the compressive stress region, under certain conditions. Also, infilling fractures are more likely to initiate near the interfaces than in the middle of the fractured layer.

We have only treated the problem in two dimensions, so one may argue that the results may not be applicable for fractures propagating in the direction perpendicular to the cross-section (horizontal propagation). In other words, a fracture may propagate horizontally and infill between two existing fractures with spacing to layer thickness ratio less than the critical value, and hence form more closely spaced fractures. However, the compressive stress exists in a cylindrical volume, if viewed in three dimensions, and this volume is as extensive as the fractures. This compression should inhibit horizontal propagation of a fracture between two existing fractures with spacing to layer thickness ratio less than the critical value.

6. Conclusions

From the study of the stress state transition between two adjacent opening-mode fractures, we have defined a critical fracture spacing to layer thickness ratio. When the fracture spacing to layer thickness ratio changes from greater than to smaller than the critical value, the normal stress in the direction perpendicular to the fractures changes from tensile to compressive. The critical spacing to layer thickness ratio increases non-linearly with increasing ratio of the Young's modulus of the fractured layer to that of the neighboring layers, with increasing Poisson's ratio of the fractured layer, and with increasing magnitude of overburden stress (depth). But, the critical ratio decreases nonlinearly with increasing Poisson's ratio of the neighboring layers. The critical spacing to layer thickness ratio provides an explanation for fracture saturation.

We have classified the joint spacing data from the literature into four ranges with Range I: $S/T_f > 1.2$; Range II: $0.8 \leq S/T_f < 1.2$; Range III: $0.3 \leq S/T_f < 1.2$; and Range IV: $S/T_f < 0.3$. Joints in Range I represent the unsaturated cases. Range II corresponds to the critical spacing to layer thickness ratio as determined from our numerical modeling. Joints in Range III and Range IV imply that another mechanism for infilling must operate. Possible mechanisms include joint initiation from flaws with finite curvature and growth of crack-like flaws driven by internal fluid pressure or overburden stress.

Acknowledgements

This research is supported by the Stanford Rock Fracture Project and the National Science Foundation grant No. EAR-9805324. We thank Atilla Aydin, Huajian Gao, Michael Gross and Gary Mavko, for their valuable discussion and suggestions, and Lisa Arrington, Drew Nelson and Ivan Nevarez, for their assistance and instruction in the experimental work. We appreciate the reviews provided by James Evans, Mark Fischer, Shaocheng Ji and Dave Sanderson.

Appendix. The Hobbs model

The Hobbs (1967) model was based on the fibre-loading theory initially outlined by Cox (1952). The fibre-loading theory considers a cylindrical fibre of one material embedded in an isotropic matrix of another, whereas the Hobbs model considers a layered system (Fig. A1). Hobbs postulated the following.

1. There is no slippage at the interfaces and all the layers are welded together.
2. All the layers have the same strain (ε_{xx}) before fracturing.
3. The elastic moduli of the two neighboring layers are E_n and G_n. They may differ from those of the fractured layer, E_f and G_f.
4. The neighboring layers have the same thickness, which is greater than that of the fractured layer, i.e. $T_n > T_f$.
5. The stress $\sigma_{xx} = E_f\varepsilon_{xx}$ in the fractured layer is independent of the vertical locations, i.e. σ_{xx} is only a function of x.
6. After the fracture formation, the stress σ_{xx} across the fracture faces is zero, and at a distance x from the fracture σ_{xx} satisfies the condition $d\sigma_{xx}/dx = 2\lambda(u_1^a - u_2^b)/T_f$, where u_1^a is the displacement in the fractured layer after fracturing, u_2^b is the displacement in the neighboring layer before fracturing, and λ is a constant related to the shear modulus of the neighboring layers.
7. The shear stress σ_{yx} in the neighboring layers decreases linearly in the vertical direction, such that $\sigma_{yx} = \sigma_{yx}^d(T_f - y)/T_f$, where σ_{yx}^d is the shear stress at the interface and a function of x only, y is the distance from the interface, and T_f is the distance in the vertical direction from the interface to where the perturbation of the stress system caused by the formation of the joint extends, which is also the thickness of the fractured layer.
8. The normal stress in the fractured layer (σ_{xx}) is balanced by the shear stress at the interface (σ_{yx}^d) in such a way that $d\sigma_{xx}/dx = 2\sigma_{yx}^d/T_f$.

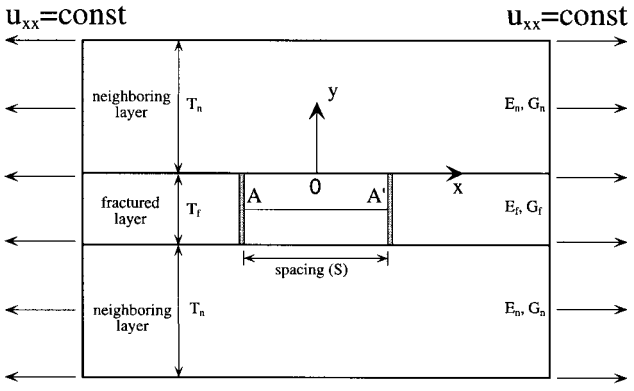

Fig. A1. Sketch diagram showing the layered model used by Hobbs (1967) in studying joint spacing in layered rocks. In his model, the neighboring layers have the same elastic constants, and the same thickness. The fractured central layer may have different elastic constants from the neighboring layers. Also it has a thickness smaller than that of the neighboring layers.

Using the above assumptions and the applied strain boundary condition shown in Fig. A1, Hobbs (1967) derived that the stress distribution between two adjacent fractures in a series of confined equally spaced fractures (Fig. A1) as being

$$\sigma_{xx} = E_f\varepsilon_{xx}(\text{ave})\left\{1 - \frac{\cosh(Dx)}{\cosh(DS/2)}\right\}, \tag{A1}$$

where $D = (2/T_f)\sqrt{G_n/E_f}$, and ε_{xx}(ave) is the average strain normal to the fractures. The solution by Hobbs (1967) provides a stress distribution between adjacent fractures that is not consistent with the solution for the full elastic boundary value problem as determined using the finite element code FRANC. To show their inconsistency, we plot the stress distributions predicted by Eq. (A1) in Fig. A2 using the same set of elastic constants as in Fig. 2, i.e. $E_f = E_n = 40$ GPa, $\nu_1 = \nu_2 = 0.2$, and the same spacing to layer thickness ratios. By comparing Figs. 2 and A2, we see that the stress magnitudes predicted by the Hobbs model are greater in general, and always tensile. Thus, the Hobbs solution fails to predict the stress state transition as the fracture spacing to layer thickness ratio changes to values less than one.

The correct solution for an elastic boundary value problem requires the use of the equilibrium and compatibility equations as well as the Hooke's law (Timoshenko and Goodier, 1970). These are the complete set of governing equations. Failure to adhere to these equations produces an erroneous stress distribution. The equilibrium equations for two-dimensional elasticity problems in the absence of body forces are

$$\frac{\partial\sigma_{xx}}{\partial x} + \frac{\partial\sigma_{yx}}{\partial y} = 0, \tag{A2}$$

$$\frac{\partial\sigma_{xy}}{\partial x} + \frac{\partial\sigma_{yy}}{\partial y} = 0, \tag{A3}$$

where $\sigma_{xy} = \sigma_{yx}$ by conservation of angular momentum (Timoshenko and Goodier, 1970).

Suppose the Hobbs solution satisfies Eq. (A2), let us see whether it satisfies Eq. (A3) in the fractured layer. Hobbs does not give an expression for the shear stress σ_{xy} nor the normal stress σ_{yy} in the fractured layer. From assumption 8, Eq. (A2) and the condition $\sigma_{yx}(y = 0) = \sigma_{yx}^d$, we have

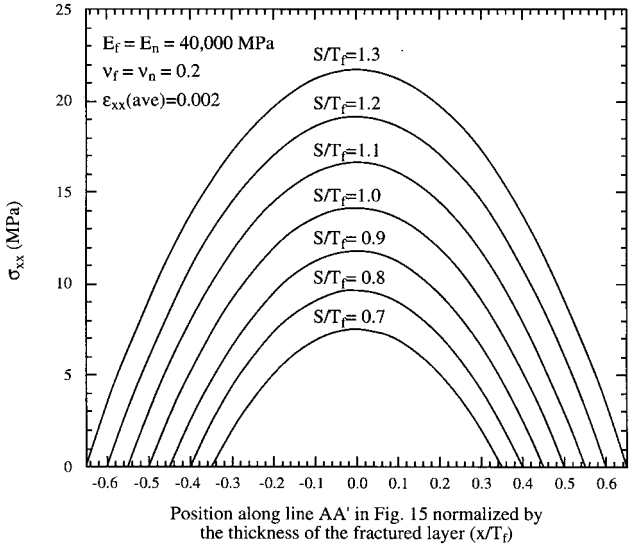

Fig. A2. Distribution of fracture normal stress between two adjacent fractures from the Hobbs model. The figure shows that the fracture normal stress (σ_{xx}) between two adjacent fractures predicted by the Hobbs model is tensile for all the spacing to layer thickness ratios.

$$\sigma_{xy} = \sigma_{yx} = \left(1 + \frac{2y}{T_f}\right)\sigma^d_{yx}, \tag{A4}$$

where σ^d_{yx} can be derived using assumption 8 and Eq. (A1) as

$$\sigma^d_{yx} = -(E_f G_n)^{1/2}\varepsilon_{xx}(\text{ave})\frac{\sinh(Dx)}{\cosh(DS/2)}. \tag{A5}$$

Eq. (A5) shows that σ^d_{yx} is a non-linear function of x. Therefore, the shear stress σ_{xy} in (A4) is a non-linear function of x and a linear function of y. Note that

$$\sigma_{yx}(x = \pm S/2, y = 0) = \sigma^d_{yx}(x = \pm S/2)$$
$$= \mp(E_f G_n)^{1/2}\varepsilon_{xx}(\text{ave})\tanh(DS/2). \tag{A6}$$

Thus Eq. (A4) does not satisfy the boundary condition at the fracture ($x = \pm S/2$), where $\sigma_{yx} = \sigma_{xy} = 0$.

If we suppose the Hobbs' solution satisfies Hooke's law, we have

$$\varepsilon_{xx} = \frac{1}{E_f}(\sigma_{xx} - \nu_f\sigma_{yy}), \tag{A7}$$

for plane stress, and

$$\varepsilon_{xx} = \frac{1-\nu_f^2}{E_f}\sigma_{xx} - \frac{\nu_f(1+\nu_f)}{E_f}\sigma_{yy}, \tag{A8}$$

for plane strain. However, Hobbs uses

$$\varepsilon_{xx} = \frac{\sigma_{xx}}{E_f}. \tag{A9}$$

From Eqs. (A7) and (A9), we have $\sigma_{yy} = 0$. From Eqs. (A8) and (A9), we have $\sigma_{yy} = -[\nu_f/(1+\nu_f)]\sigma_{xx}$, which is independent of y. Thus, in both cases, we get $\partial\sigma_{yy}/\partial y = 0$, whereas Eq. (A4) implies that $\partial\sigma_{xy}/\partial x$ is a non-linear function of x. Therefore, the Hobbs solution does not satisfy Eq. (A3) in the fractured layer.

In the neighboring layers, $\sigma_{xx} = E_n\varepsilon_{xx}(\text{ave}) = \text{constant}$, whereas σ_{yx} is a linear function of y (assumption 7), i.e. $\partial\sigma_{xx}/\partial x = 0$ but $\partial\sigma_{yx}/\partial y = \text{constant}$. Thus, Eq. (A2) is not satisfied in the neighboring layers.

From the above analysis, we conclude that the solution by Hobbs (1967) does not satisfy the complete set of governing equations of elasticity, and suggest that this solution should be abandoned. However, the conceptual model Hobbs proposed for stress transfer from neighboring layers and sequential infilling has merit. Indeed, the FEM solution we utilize includes such stress transfer and admits the development of additional fractures by sequential infilling. This process is limited by the transition from tension to compression when $S/T_f \approx 1.0$, and this transition is not found in the Hobbs solution.

References

Bai, T., Pollard, D.D., Gross, M.R., in press. Mechanical prediction of fracture operture in layered rocks. Journal of Geophysical Research.

Barber, J.R., 1992. Elasticity. In: Gladwell, G.M.L. (Ed.), Solid Mechanics and its Applications, vol. 12. Kluwer, London 293 pp.

Becker, A., Gross, M.R., 1996. Mechanism for joint saturation in mechanically layered rocks: an example from southern Israel. Tectonophysics 257, 223–237.

Biot, M.A., 1965. Mechanics of Incremental Deformation. John Wiley, New York 519 pp.

Bogdanov, A.A., 1947. The intensity of cleavage as related to the thickness of beds. Soviet Geology 16 (in Russian).

Cherepanov, G.P., 1997. On the origin of joints in sedimentary rocks. In: Karihaloo, B.L., Mai, Y.-W., Ripley, M.I., Ritchie, R.O. (Eds.), Advances in Fracture Research, Proceedings of the Ninth International Conference of Fracture, Sydney, Australia, vol. 4, pp. 1757–1766.

Cobbold, P.R., 1979. Origin of periodicity: saturation or propagation? Journal of Structural Geology 1, 96.

Cox, H.L., 1952. The elasticity and strength of paper and other fibrous materials. British Journal of Applied Physics 3, 72–79.

Dundurs, J., 1969. Discussion on edge bonded dissimilar orthogonal elastic wedges under normal and shear loading. Journal of Applied Mechanics 36, 650–652.

Garrett, K.W., Bailey, J.E., 1977a. Multiple transverse fracture in 90° cross-ply laminates of a glass fibre-reinforced polyester. Journal of Materials Science 12, 157–168.

Garrett, K.W., Bailey, J.E., 1977b. The effect of resin failure strain on the tensile properties of glass fibre-reinforced polyester cross-ply laminates. Journal of Materials Science 12, 2189–2194.

Gross, M.R., 1993. The origin and spacing of cross joints: examples from Monterey Formation, Santa Barbara Coastline, California. Journal of Structural Geology 15, 737–751.

Gross, M.R., Engelder, T., 1995. Fracture strain in adjacent units of the Monterey Formation: Scale effects and evidence for uniform

displacement boundary conditions. Journal of Structural Geology 17, 1303–1318.

Gross, M.R., Fischer, M.P., Engelder, T., Greenfield, R.J., 1995. Factors controlling joint spacing in interbedded sedimentary rocks: integrating numerical models with field observations from the Monterey Formation, USA. In: Ameen, M.S. (Ed.), Fractography: Fracture Topography as a Tool in Fracture Mechanics and Stress Analysis, Geological Society Special Publication No. 92, pp. 215–233.

Gross, M.R., Bahat, D., Becker, A., 1997. Relations between jointing and faulting based on fracture-spacing ratios and fault-slip profiles: A new method to estimate strain in layered rock. Geology 25, 887–890.

Hatheway, A.W., Kiersch, G.A., 1989. Engineering properties of rock. In: Carmichael, R.S. (Ed.), Practical Handbook of Physical Properties of Rocks and Minerals. CRC Press, Boca Raton, FL, pp. 672–715.

Helgeson, D.E., Aydin, A., 1991. Characteristics of joint propagation across layer interfaces in sedimentary rocks. Journal of Structural Geology 13, 897–911.

Hobbs, D.W., 1967. The formation of tension joints in sedimentary rocks: an explanation. Geological Magazine 104, 550–556.

Huang, Q., Angelier, J., 1989. Fracture spacing and its relation to bed thickness. Geological Magazine 126, 355–362.

Jaeger, J.C., Cook, N.G.W., 1979. Fundamentals of Rock Mechanics, 3rd ed. Chapman & Hall, London 539 pp.

Ji, S., Saruwatari, K., 1998. A revised model for the relationship between joint spacing and layer thickness. Journal of Structural Geology 20, 1495–1508.

Ji, S., Zhao, P., 1994. Strength of two-phase rocks: a model based on fibre-loading theory. Journal of Structural Geology 16, 253–262.

Kirillova, I.V., 1949. Some problems of the mechanics of folding. Trans. Geofian. 6 (in Russian).

Lachenbruch, A.H., 1961. Depth and spacing of tension cracks. Journal of Geophysical Research 66, 4273–4292.

Ladeira, F.L., Price, N.J., 1981. Relationship between fracture spacing and bed thickness. Journal of Structural Geology 3, 179–183.

Lloyd, G.E., Ferguson, C.C., Reading, K., 1982. A stress-transfer model for the development of extension fracture boudinage. Journal of Structural Geology 4, 355–372.

Masuda, T., Kuriyama, M., 1988. Successive 'mid-point' fracturing during microboudinage: an estimate of the stress–strain relation during a natural deformation. Tectonophysics 147, 171–177.

Masuda, T., Shibutani, T., Igarashi, T., Kuriyama, M., 1989. Microboudin structure of piedmontite in quartz schists: a proposal for a new indicator of relative paleodifferential stress. Tectonophysics 163, 169–180.

Masuda, T., Shibutani, T., Kuriyama, M., Igarashi, T., 1990. Development of microboudinage: an estimate of changing differential stress with increasing strain. Tectonophysics 178, 379–387.

McQuillan, H., 1973. Small-scale fracture density in Asmari Formation of southwest Iran and its relation to bed thickness and structural setting. American Association of Petroleum Geologists Bulletin 57, 2367–2385.

Narr, W., Lerche, I., 1984. A method for estimating subsurface fracture density in core. American Association of Petroleum Geologists Bulletin 66, 637–648.

Narr, W., Suppe, J., 1991. Joint spacing in sedimentary rocks. Journal of Structural Geology 13, 1037–1048.

Novikova, A.C., 1947. The intensity of cleavage as related to the thickness of the bed. Soviet Geology 16 (in Russian).

Nur, A., 1982. The origin of tensile fracture lineaments. Journal of Structural Geology 4, 31–40.

Parvizi, A., Bailey, J.E., 1978. On multiple transverse cracking in glass fibre epoxy cross-ply laminates. Journal of Materials Science 13, 2131–2136.

Pollard, D.D., Aydin, A., 1988. Progress in understanding jointing over the past century. Geological Society of America Bulletin 100, 1181–1204.

Pollard, D.D., Segall, P., 1987. Theoretical displacements and stresses near fractures in rocks: with applications to faults, joints, veins, dikes and solution surfaces. In: Atkinson, B.K. (Ed.), Fracture Mechanics of Rock. Academic Press, London, pp. 277–349.

Price, N.J., 1966. Fault and Joint Development in Brittle and Semi-Brittle Rocks. Pergamon Press, Oxford 176 pp.

Rives, T., Razack, M., Petti, J.P., Rawnsley, K.D., 1992. Joint spacing: analogue and numerical simulations. Journal of Structural Geology 14, 925–937.

Sowers, G.M., 1972. Theory of spacing of extension fracture. In: Pincus, H. (Ed.), Engineering Geology Case History Number 9: Geological Factors in Rapid Excavation. The Geological Society of America, Engineering Geology Division, pp. 27–52.

Timoshenko, S.P., 1936. Theory of Elastic Stability. McGraw-Hill, New York 495 pp.

Timoshenko, S.P., Goodier, J.N., 1970. Theory of Elasticity, 3rd ed. McGraw-Hill, New York 567 pp.

Wawrzynek, P.A., Ingraffea, A.R., 1987. Interactive finite element analysis of fracture processes: An integrated approach. Theoretical and Applied Fracture Mechanics 8, 137–150.

Wu, H., Pollard, D.D., 1991. Fracture spacing, density, and distribution in layered rock masses: results from a new experimental technique. In: Toegiers, J.-C. (Ed.), Rock Mechanics as a Multidisciplinary Science, Proc. 32nd U.S. Symposium on Rock Mechanics. Balkema, Rotterdam, pp. 1175–1184.

Wu, H., Pollard, D.D., 1992. Propagation of a set of opening-mode fractures in layered brittle materials under uniaxial strain cycling. Journal of Geophysical Research 97, 3381–3396.

Wu, H., Pollard, D.D., 1995. An experimental study of the relationship between joint spacing and layer thickness. Journal of Structural Geology 17, 887–905.